Title

Electrochemically Triggered Pore Expansion in Nanoporous Gold Thin Films

Permalink

https://escholarship.org/uc/item/60h4g9fr

Journal

The Journal of Physical Chemistry C, 120(7)

ISSN

1932-7447

Authors

Dorofeeva, Tatiana S
Matharu, Zimple
Daggumati, Pallavi
et al.

Publication Date

2016-02-25

DOI

10.1021/acs.jpcc.5b11268

Peer reviewed

Article

Electrochemically-Triggered Pore Expansion in Nanoporous Gold Thin Films

Tatiana Dorofeeva, Zimple Matharu, Pallavi Daggumati, and Erkin Seker

Just Accepted

Electrochemically-Triggered Pore Expansion in

Nanoporous Gold Thin Films

Tatiana S. Dorofeeva, Zimple Matharu, Pallavi Daggumati, Erkin Seker*

Department of Electrical and Computer Engineering, University of California - Davis,

Davis, CA 95616, USA

*Corresponding author: eseker@ucdavis.edu

ABSTRACT

Nanoporous electrode coatings have played a significant role in enhancing the performance of catalysts and sensors. For optimal performance in these applications, the fundamental requirement is a large effective surface area (site at which catalysis and sensing events occur) with unhindered transport of reactants and products to/from the active surface. This necessitates low-density porous electrodes with an interconnected 3D network of thin conductive ligaments to maintain high effective surface area. While the logical approach to create such electrodes is to etch the ligaments uniformly through the entire porous network, accomplishing this has not been trivial. Here, we use nanoporous gold (np-Au) as a model material system to demonstrate an electrochemically-triggered etching method for restructuring sputter-deposited sub-micron np-Au thin films for enlarging the pores with minimal decrease in the effective surface area. We systematically employ time-varying potential waveforms to electrochemically modify morphologies and reveal underlying mechanisms of the etching process. The results suggest that the etch cycle at positive potentials plays a dual role of electrophoretic attraction of chloride ions and initiating the electrochemical etch. The final nanoporous morphology is dictated by a competition between ligament coarsening and ligament thinning, which provide a means to generate a wide range of electrode morphologies.

INTRODUCTION

Recent advances in material science and chemistry have enabled the development of a wide range of nanostructured materials with unique characteristics such as increased surface area-to-volume ratio, enhanced electro-catalytic activity, and intriguing optical, mechanical, electrical, and biological properties[1-4]. Nanoporous metals (e.g., gold[5], silver[6], platinum[7], copper[8]) produced by a selective alloy corrosion process, commonly referred to as *dealloying*, exhibit a three-dimensional interconnected open-pore structure[2, 9]. During the dealloying process, a less noble constituent (e.g., silver) of an alloy (e.g., silver-rich gold) is removed, while the noble metal atoms diffuse at the metal-electrolyte interface to form the nanoporous structure. The large surface area-to-volume ratio, electrical conductivity, and tunable morphology of nanoporous metals make them ideally suited for sensor[10-11], energy conversion[12], and energy storage applications[13]. Nanoporous metals are also promising candidates as electrodes in electrochemical capacitors[14], where they can store orders of magnitude more electrical charge compared to traditional capacitors. However, enhanced effective surface area alone is not sufficient for desired high charge/discharge rates, as the ionic transport to the surface is generally hindered[15]. Taken together, a fundamental requirement for optimal performance of catalysts, ultra-capacitors, and sensors is to have a large surface area per unit footprint or unit volume while also maintaining unhindered access to the active surface[2]. The effective surface area of a nanoporous geometry scales inversely with its characteristic size of the geometric features (i.e., ligaments and pores, see inset in Figure 1A for the definitions); however, small pores typically impede mass transport to the ligament surfaces within the porous network. Therefore, in order to take advantage of the enhanced effective surface, the pores need to be large enough to facilitate mass transport. Unfortunately, achieving this is not a trivial task. Almost exclusively all methods to date (e.g., thermal[16], electrochemical[17-18], electro-thermal[19], photo-thermal[20-21]) enhance surface diffusion of the noble element, leading to a ligament coarsening event and consequently enlarged pores. While the latter is desirable from a mass

transport perspective, coarsened ligaments reduce effective surface area. Currently, all of the aforementioned methods lack the ability to decouple pore expansion from ligament coarsening.

In order to address the shortcomings of the conventional annealing processes, we report electrochemical etching (also referred to as *ligament thinning*) as a novel process that enlarges the pores (better accessibility) while minimally impacting the effective surface area. As a model system for nanoporous metals produced by dealloying, we use nanoporous gold (np-Au), which has been the most popular material system as it embodies numerous advantages, including high electrical conductivity[22], compatibility with microfabrication processes[19], well-established gold-thiol chemistry for surface functionalization[23], tunable mechanical properties[24-25], and biocompatibility[26]. By employing electrochemical etching at time-varying potentials, we probe the underlying etch mechanisms and discuss its implications to catalysis and sensing applications.

EXPERIMENTAL SECTION

Chemicals/Materials

Glass coverslips (24 x 24 mm, thickness 0.13 - 0.16 mm) were purchased from Fisher Scientific. Piranha solution, used for cleaning the coverslips, consisted of 1:4 mixture of hydrogen peroxide (concentration 30%) and sulfuric acid (concentration 96%) from J. T. Baker. Metal targets (chromium, gold, and silver of 99.95% purity) were purchased from Kurt J. Lesker. Nitric acid (70%) from Sigma-Aldrich was used for dealloying. Hydrochloric acid (HCl) (40%) used for electrochemical etching was purchased from J. T. Baker.

Sample Preparation

Glass coverslips (24 x 24 mm) were cleaned in piranha solution for 7 minutes, rinsed in deionized (DI) water and dried. An adhesion layer of 120 nm-thick chrome and 80 nm-thick intermediate gold layer were sputter-deposited prior to the depositing the 500 nm-thick gold-

silver alloy (silver 65% and gold 35%) layer. Dealloying was performed by immersing the samples in 70% nitric acid heated to 55 ºC for 15 minutes. Samples were soaked in DI water for 2 days to remove any residual nitric acid. Detailed sample fabrication and preparation process is described in our previous work[27].

Electrochemical Methods

Coverslips were cut into 6 x 24 mm samples. Electrochemical etching was performed by immersing approximately 12 mm of the np-Au sample in a mixture of hydrochloric acid and water (1:4 ratio by volume). A potentiostat (PalmSens) in a 2-electrode configuration was used to apply positive voltage to the np-Au sample (working electrode), while platinum wire served as an anode (counter electrode). All potentials indicated in the manuscript are with respect to the platinum electrode. Pulse amperometry mode was used to study the influence of pulse duration, pulse frequency, and pulse magnitude on the electrochemical etching processes. As the potentiostat did not have high frequency (>20 Hz) capability in the pulse amperometry mode, we used a function generator in a separate experiment for three different frequencies (1, 10, 100 Hz). The effective surface area of samples was determined by cyclic voltammetry (CV) in 50 mM H_2SO_4 at a scan rate of 50 mV/s, as previously demonstrated[23, 27-28]. Surface area *enhancement factor* is defined as a ratio between effective surface area of np-Au samples and effective surface area of planar gold samples.

Morphological Characterization

Samples were characterized by obtaining top and cross-sectional scanning electron microscope (SEM) images using FEI Nova NanoSEM430. Top views were converted to binary images and ligament and pore sizes were calculated using custom MatLab scripts and ImageJ software, using methods previously described[19].

RESULTS AND DISCUSSION

Electrochemical Etching Process

In order to emphasize the need for the electrochemical etching, it would be helpful to describe the challenge in employing traditional open-potential chemical etching of a high-aspect ratio material, such as np-Au. If np-Au is immersed in a traditional iodine-based gold etchant, the etchant permeates the porous structure and begins to etch the ligaments. However, the etch process is difficult, if not impossible, to control, because once etchant gets into the pores, the etching proceeds quickly leading to removal of the entire porous film. It is not possible to quench the etching by immediate immersion into a rinsing medium (e.g., DI water), as it takes considerable time for molecules to leave the porous structure, as shown previously[27]. Electrochemical etching on the other hand is ideally suited for this task because it is possible to immerse np-Au in a solution (HCl and water) which does not etch unless a critical electrochemical potential is administered. In this process, hydrochloride dissociates in water, resulting in an ample supply of free chloride anions[29]. When an appropriate positive potential is applied to the gold working electrode, gold atoms oxidize and react with chloride anions[30] (electrochemical setup illustrated in Figure S1A). This reaction prevents gold atoms from redepositing on the surface. Chloroaurate complexes then diffuse away from the anode, giving way for fresh chloride ions to react with oxidized gold atoms[31]. Figure 1 depicts the top and cross-sectional SEM images for electrochemically-etched np-Au electrodes along with un-etched control electrodes (ctrl). Top-view of the etched np-Au sample contains larger pores (indicative of enhanced accessibility to the porous network underneath). Pore area coverage for etched samples (such as the one shown in Figure 1B), obtained from image analysis on 20 different samples, was 46%± 3.8% (mean±standard deviation). While for control samples pore area coverage was 29%±3.5%. The small standard deviations highlight the reproducibility of the

ligament thinning and dealloying processes respectively. Cross-sectional SEM images revealed that the film thickness decreased slightly with etching and that ligaments were uniformly thinned through the entire film thickness. The initial film thickness was approximately 520 nm and it decreased by approximately 65 nm for moderately etched samples (Figure 1), confirming the etching uniformity. The morphology across the etched region was also highly uniform (Figure S2).

We initially investigated how the concentration of chloride ions and potential supplied to the electrode impacts the final film morphology. Although several different concentrations from 1:2 to 1:11 were initially investigated, where all the ratios indicate ratio of volumetric HCl to volumetric H_2O. Higher concentrations of 1:2 ($HCl:H_2O$) resulted in more rapid etching while lower concentrations of 1:11 resulted in much longer etch times to obtain comparable ligament thickness (Figure S3). Cyclic voltammetry studies were used to determine the critical potential for the etching process. We observed an oxidation peak with abrupt increase in current around 1.1 V (Figure S1C), thus 1.1 V was selected as the etching potential (V_{on}) for all etching experiments, no etching was observed at potentials below 1.1 V (Figure S4). Substantial etching of np-Au samples was always accompanied by a noticeable color change as shown in supplementary information (Figure S1A).
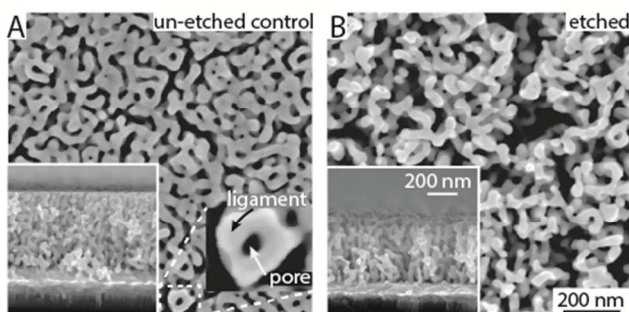
Figure 1. Top view of A) un-etched control (ctrl) and B) etched samples. Cross-sectional images corresponding to each top view are shown in the insets. The electrochemical etching is uniform through

the film thickness and pore area coverage expands while ligament coarsening is limited. Designation of ligament (gray areas) and pore (dark areas) is illustrated in the inset of main image A).

Etching at Constant Potential

We initially performed the etching at a constant potential to demonstrate the concept of electrochemical etching. The sample was first held at open circuit potential (OCP), which was close to 0 V, where there was no etching observed. Subsequently, 1.1 V was applied to initiate etching. Etch durations (t_{etch}) of 2.5, 5, 10, 20, and 40 seconds were studied and the corresponding SEM images are shown in the Figure 2A. The voltage was then switched to OCP to terminate the etching. In order to define the nomenclature for potential waveform components used in this paper, a representative plot of applied voltage versus time for a 3 s etching process is illustrated in the Figure 2B. The image analysis revealed that the pore coverage increased by approximately 9% (compared to the control sample) for the 2.5 s etch. Pore coverage continued to increase, reaching a maximum of 18% for an etch duration of 10 s (Figure 2C). For longer etch durations (represented by the 20 s sample) extensive gold etch resulted in ligament separation into individual surface-bound fibers that are prone to surface tension-driven aggregation upon drying, which ultimately decreases the overall pore coverage. Continued etching to as long as 40 s resulted in almost complete removal of np-Au layer. It should be noted that the light-colored regions in Figure 2A (40 s) are vestiges of the ligaments and not the pores. However, image analysis designates darker areas as pores resulting in dramatically higher pore coverage estimation (shaded column in Figure 2C). Although constant potential etching provides an effective and simple means to controllably thin the ligaments of np-Au thin films, it does not reveal the dynamics of underlying mechanisms and time scales of the etching process, which is composed of diffusion- and reaction-driven components. A fundamental understanding of these processes is necessary for rational engineering of different pore morphologies for specific applications.
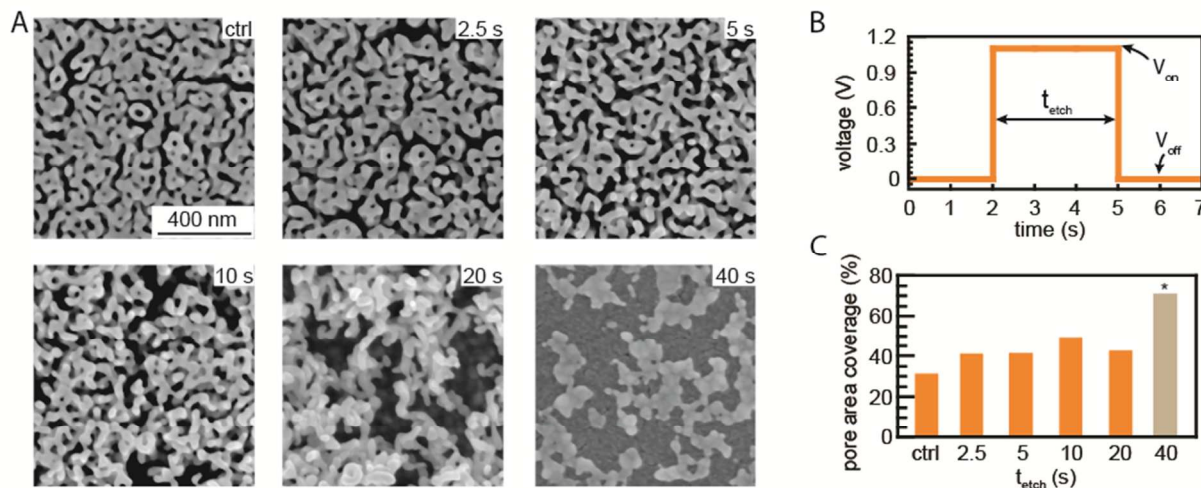
Figure 2. A) Constant-potential etching V_{on} = 1.1 V, V_{off} = 0 V, etch times t_{etch} = 0, 2.5, 5, 10, 20, 40 s. B) Plot illustrates the applied potential versus time. For the example curve in this plot, t_{etch} = 3 s, V_{on} = 1.1 V, and V_{off} = 0 V. C) Pore area coverage (indicative of accessibility) obtained from SEM images on the left. *Majority of the np-Au layer was removed for the 40 s case, thus results of image analysis do not represent pore area coverage but rather the percent area of the underlying substrate exposed after etching.

Etching at Time-Varying Potentials

The complete electrochemical etching cascade involves several processes, including transport of Cl⁻ ions to ligament surfaces within the porous structure, reaction with oxidized gold atoms, and transport of products away from the ligaments. The interplay of these processes leads to the generation of a wide range of morphologies. By systematically varying the potential waveform used for etching, here we aim to decouple mass transport and reaction components of the etching process. An example of the time-varying etching potential is shown in Figure 3B. The time-varying etching potential signal consists of a series of pulses where etching only proceeds when at 1.1 V (V_{on}), while no etching occurs at OCP or 0 V (V_{off}). The width of the pulses and duration between the pulses can be independently varied (see frequency and *on* and *off* study below). For this study both the pulse width (t_{on}) and *off* duration (t_{off}) were set to 0.5 s (frequency=1 Hz). Total etch time was obtained by multiplying the number of pulses by the

duration of a single pulse, as etching only takes place at V_{on}. For example, an experiment duration of 40 s resulted in an effective etch time of 20 s (shown in Figure 3B). While we did not observe significant differences for time-varying and constant potential etching methods (see supporting information Figure S5 for SEM images comparing constant and time-varying etching), the time-varying method offers additional parameters necessary for investigating the etching process in detail by decoupling transport and reaction mechanisms.

Effect of Pulse Frequency on Etching

We investigated the effect of frequency (i.e., 1, 10, 100 Hz) on the etching process to provide insight into the time scales of the underlying mechanisms (i.e., mass transport vs. reaction). Although the effective etch duration, that is, the time spent when the potential was on, is equal for all cases (15 s), less etching was observed with increasing frequency (Figure 3A). We hypothesized that in the case of constant potential or frequencies lower than 1 Hz, the mass transport and reaction times are shorter than the *on* and *off* times of each cycle. This, in turn, allows for sufficient time for reactants to permeate the pores, react with the ligament surfaces, and for products to exit the pores (see constant/time-varying potentials (f < 1 Hz) in Figure 3C). As frequency increases, either t_{on} becomes shorter than the reaction time ($t_{on} < t_{reaction}$) and reactants have no time to react, or, t_{off} is not sufficient to transport the reactants into and products away from the ligaments surfaces ($t_{off} < t_{transport}$), thus yielding less etching, as judged by similar appearance to the *control* sample (Figure 3A).
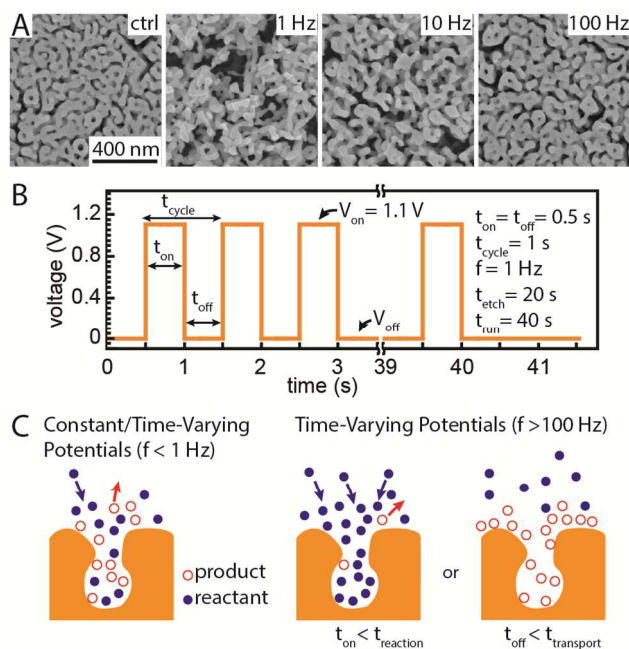
Figure 3. A) Comparison of morphologies obtained while varying the frequency of the pulses during time-varying etching: For all cases V_{on}=1.1 V and V_{off}=0 V and t_{etch}=15 s. Frequencies investigated were 1, 10 and 100 Hz. B) Plot illustrating the voltage variation with time for the time-varying etching process. For the etching potential waveform illustrated here, the pulse width and the *off* times are equal and each cycle is 1 s long. This results in total etch time of 20 s. V_{on}=1.1 V and V_{off}=0 V. C) Illustration of etching process during constant and time-varying etching: During constant or time-varying etching at low frequencies <1 Hz, the mass transport and reaction times are shorter than *on* and *off* times of each cycle, thus significant etching is observed. During time-varying etching at higher frequencies >100 Hz, either reaction time is longer than pulse duration or the *off* time is not sufficient for reactants and products to move in and out of the pore, resulting in minimal etching.

Effect of t_{on} and t_{off} on Etching

In order to determine whether the mass transport or reaction times dictate the electrochemical etching outcome, the etch parameters, t_{on} and t_{off}, were varied independently to study the two components (i.e., transport and reaction) separately. Four cases were investigated. Based on the results of the frequency study, less etching was observed at 10 Hz compared to 1 Hz, these two frequencies were used as reference baselines in this study. At 10 Hz (case ii) both t_{on} or t_{off}

are shorter than the corresponding times at 1 Hz (case i). Hence it is unclear whether t_{on} played

a dominant role in dictating the final morphology or t_{off}. In the other two cases, we decoupled t_{on}

and t_{off}. The third case combined t_{on} from 1 Hz case and t_{off} from 10 Hz case (case iii, 0.5 / 0.05

s), and final case used t_{on} from 10 Hz and t_{off} from 1 Hz (case iv, 0.05 / 0.5 s). The SEM images

of morphologies obtained for each case are shown in Figure 4A. From the SEM images, the

morphologies for 1 Hz (case i) and t_{on}=0.5 s (case iii) were comparable and pore coverage for

both increased by 15% over the control samples. The other two cases (ii and iv) also exhibited a

similar morphology; however, the pore area coverage increased by only 7% over the control

samples (Figure 4B). From the images, it is obvious that t_{on} plays the most significant role in the

etch process. These results suggest that the critical transport time of reaction products must be

much smaller than the reaction time, since otherwise the morphology of the sample with shorter

t_{off} (case iii) should have approached the morphology in the 10 Hz (case ii) and the sample with

longer t_{off} (case iv) should have produced morphology similar to that for the 1 Hz (case i). Taken

together, the results of this study indicate that less etching at higher frequency is a result of

shorter t_{on} (Figure 4C) making it an extremely sensitive parameter which can be used to tailor

final pore size, while t_{off} (passive diffusion of reactants/products to/from the ligament surfaces)

has little impact on the final morphology.
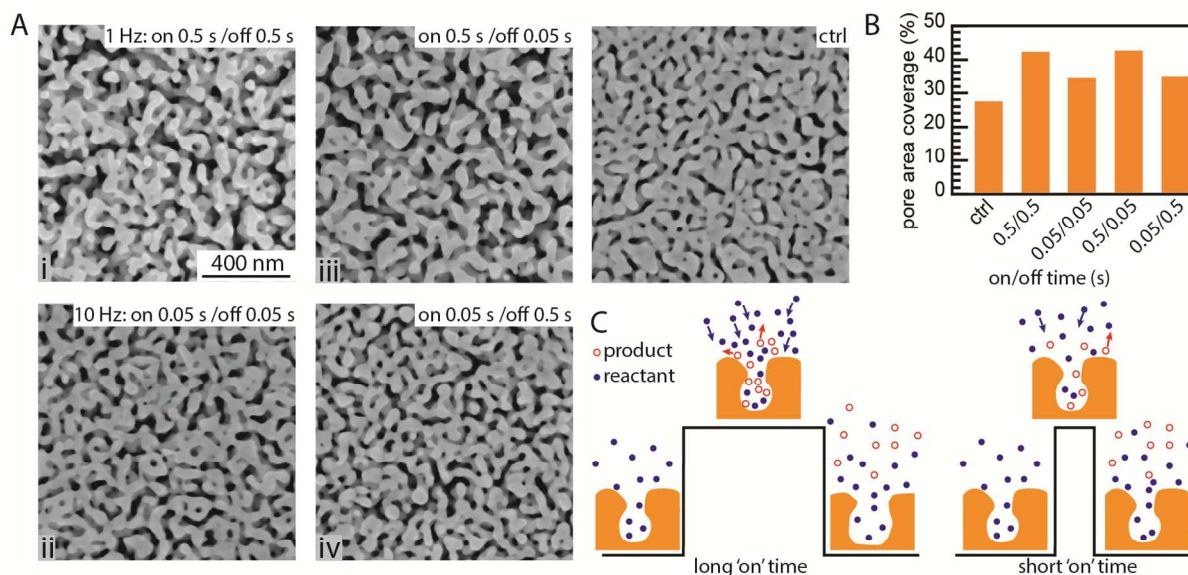
Figure 4. A) Comparison of morphologies while varying t_{on} and t_{off}. For all cases V_{on}=1.1 V and V_{off}=0 V and t_{etch}=10 s. B) Bar graph illustrating the difference in pore area coverage for the four etching regimens. C) Schematic illustration of the influence of long and short pulse width on the etching process. Initially no potential is applied and no reaction takes place. Then potential is switched to 1.1 V for t_{on}. For a long t_{on}, reactants enter the pore, reaction takes places resulting in substantial etching, and this continues until the potential is turned off. For a short t_{on}, there is not sufficient time for reactants to arrive at the ligament surface and participate in etching reaction, and thus little etching is observed. After potential is switched back to zero, products are free to exit the pore and new reactants to enter the pore.

Decoupling Reaction versus Transport Contributions to the Etch

The mass transport component of the etch process can be studied by varying the supply of Cl^- ions available for the reaction. This can be accomplished by varying the *off* voltage (V_{off}). When V_{off} is positive, the negatively charged chloride ions are electrophoretically driven to the ligament surfaces, resulting in an ample supply of ions for the reaction. On the other hand, negative V_{off} results in a deficit of chloride ions because they are repelled from the electrode surface, which should result in minimal ligament thinning. In this study we investigated three starting potentials (V_{off}): -0.7, 0, +0.7, while V_{on} remained at 1.1 V for all 3 cases (Figure 5A). The frequency in all

cases was kept at 1 Hz with an effective etch time (t_{etch}) of 15 s. The extent of ligament thinning following the etch process was comparable for V_{off}=0 and V_{off}=+0.7 V cases (Figure 5B). However, minimal etching was observed for V_{off}=-0.7 V. The pore area coverages for V_{off}=0 and V_{off}=+0.7 V cases were nearly identical (50% in contrast to 32% for the control samples); however, for the case of V_{off}=-0.7 V, the pore area coverage was less than 40%. This decrease can be justified by electrophoretic repulsion of negatively-charged chloride ions from the np-Au ligaments when V_{off} is negative. The slight coarsening observed for this case (Figure 5C) can be attributed to enhanced surface diffusion of gold atoms in the presence of adsorbed Cl⁻ ions and applied potential[2, 9, 32]. It is probable that the surface diffusion-driven ligament coarsening is also present in all cases and competes with the etching process. For the cases where substantial etching occurs, the ligaments erode as the removal of the gold atoms from the ligament (etching process) is faster than the surface diffusion of gold atoms (coarsening process). If supply of Cl⁻ ions is limited, not all diffused atoms can be removed resulting in a net coarsening of the ligaments. The combination of these two mechanisms provides an opportunity to tune morphology by controlling the polarity of the applied potential.
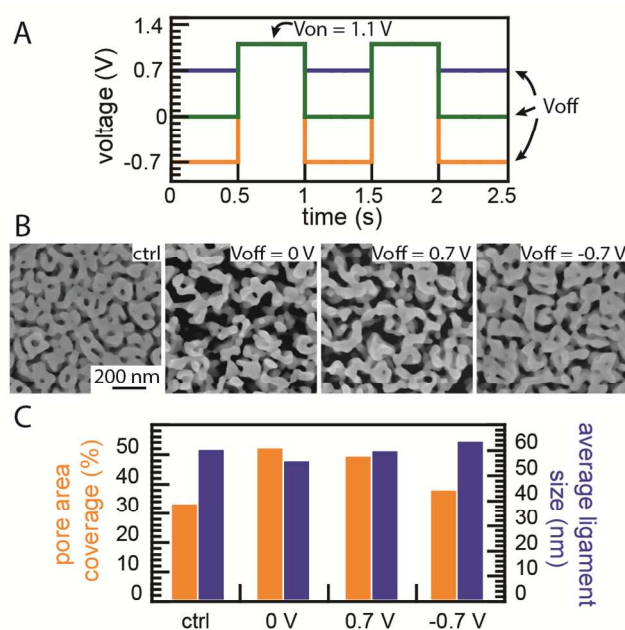
Figure 5. A) Plot illustrating voltage pulses for different test conditions. B) SEM images of the samples with morphologies modified by different V_{off} potentials while all other etch parameters were kept the same (i.e., V_{on}=1.1 V, t_{etch}=15 s, and f=1 Hz). C) Bar graph showing the percent pore coverage and average ligament size for each test condition.

Electro-chemical Etching versus Thermal Treatment

The collective morphological analysis of all electrochemical etching experiments discussed above indicates that ligament thickness slightly decreases while pore area coverage increases after the etching process. This implies that surface area should be less impacted compared to other traditional coarsening techniques, where both ligament and pore dimensions increase and consequently the effective surface area dramatically decreases. In order to assess the effectiveness of electrochemical etching in preserving surface area, we summarized the evolution of pore area coverage versus mean ligament size for electrochemical etching and thermal annealing (conducted at various temperatures ranging between 150 and 300 ºC) in Figure 6. Comparison of morphologies obtained by the two techniques revealed an interesting trend. The morphology obtained by thermal annealing showed a substantial increase in ligament thickness while pore coverage remained around 30%, as commonly observed for any conventional coarsening process[16, 19-21, 28, 33-35]. In this scenario, the surface diffusion-mediated coarsening leads to both pore and ligament growth; however, overall pore coverage does not change because ligaments simply rearrange to a more stable coarsened structure. In contrast, the morphology obtained through the electrochemical etching technique, displayed a slight decrease in ligament thickness while pore area coverage increased considerably with etching. Unlike the coarsening process, here the pore growth is due to removal of the material from the ligament.

As seen in Figure 6 inset, where surface area enhancement factor is plotted against average pore size for both techniques, as pores get larger, the enhancement factor decreases as expected. In the thermal coarsening case, the decrease in the surface area is due to number of

1
2
3
4
5
6
7
8
9
10
11
12
13
14
15
16
17
18
19
20
21
22
23
24
25
26
27
28
29
30
31
32
33
34
35
36
37
38
39
40
41
42
43
44
45
46
47
48
49
50
51
52
53
54
55
56
57
58
59
60

ligaments decreasing as they coalesce together into more stable thicker ligaments. In the case of electrochemical etching, ligament evolution goes through two stages. Initially, the decrease in surface area is due to gold atoms rearranging and ligaments becoming thinner as gold atoms are removed, thus slightly decreasing the overall surface area. At the later stages of the etching process, as more material is removed, number of ligaments starts to decrease as they collapse, further reducing the surface area. While it is not possible to obtain higher enhancement factor than the control samples (unless both pore and ligament sizes are shrunk simultaneously), electrochemical etching is clearly superior to thermal annealing in preserving the surface area while at the same time opening up the pores for improved accessibility to the surfaces within the porous structure, where the both catalysis and sensing events take place. The results show that enhancement factor for electrochemically etched np-Au samples is approximately 25% higher compared to that for thermal coarsening. For the same enhancement factor, electrochemical etching results in up to two times bigger pore size, which can be important in applications that require large surface area coupled with larger pores for improved transport of material in and out of the pores[23, 36].
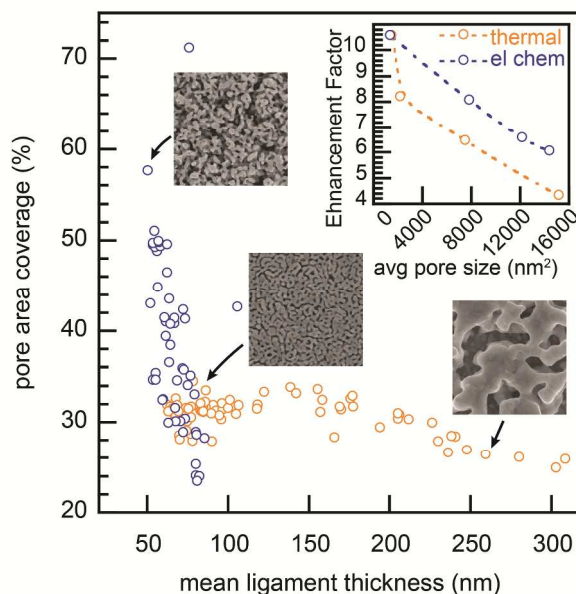
Figure 6. Comparison of ligament thickness and pore area coverage for coarsening and etching techniques. Magnification of SEM images is the same and each image displays approximately 1.2 x 1.2 µm area. Inset: Enhancement factor versus average pore size for thermal and electrochemical techniques, demonstrating that for a given enhancement factor the pore size is up to two times higher using the electrochemical technique.

CONCLUSION

We demonstrated electrochemical etching as a novel method to controllably modulate morphologies of np-Au thin films that results in larger pore sizes while limiting surface area reduction. The advantage of this technique is that no etching occurs before a critical potential is imposed, thereby allowing for unprecedented control of the etching process. In addition, the electrochemically-triggered approach offers a rich set of parameters (e.g., tunable potential waveform) to invoke mass transport- and reaction-driven components of the etch process, thereby allowing for the generation of unique morphologies. The systematic studies involving modulation of the potential waveform revealed that the etch cycle at positive potentials plays a dual role of electrophoretic attraction of chloride ions and initiating the electrochemical etch. In

addition, we isolated two competing processes (i.e., coarsening, etching) that occur during the electrochemical etching that are based on the *off* voltage and the durations of *on* and *off* etch times. Contrary to the traditional morphology coarsening approaches, this method increases pore size (favoring mass transport) while minimally affecting the effective surface area (preserving reaction sites). In combination with np-Au compatibility with microfabrication processes, this technique can be extended to create multiple electrode arrays that display different morphologies for studying structure-property relationships and tuning catalysts/sensors for optimal performance.

ACKNOWLEDGEMENT

Supporting Information. Details regarding sample preparation, experimental setup and morphological comparison between different techniques. This information is available free of charge via the Internet at http://pubs.acs.org.

REFERENCES

1.   Huber, P., Soft Matter in Hard Confinement: Phase Transition Thermodynamics, Structure, Texture, Diffusion and Flow in Nanoporous Media. *J. Phys.: Condens. Matter* **2015**, *27*, 103102.

2.   Ding, Y.; Zhang, Z., Nanoporous Metals. In *Springer Handbook of Nanomaterials*, Vajtai, R., Ed. Springer Berlin Heidelberg: 2013.

3.   Zhang, J.; Li, C. M., Nanoporous Metals: Fabrication Strategies and Advanced Electrochemical Applications in Catalysis, Sensing and Energy Systems. *Chem. Soc. Rev.* **2012**, *41*, 7016-7031.

4.   Wittstock, A.; Biener, J.; Erlebacher, J., *Nanoporous Gold: From an Ancient Technology to a High-Tech Material*; Royal Society of Chemistry, 2012.

5.   Ding, Y.; Kim, Y. J.; Erlebacher, J., Nanoporous Gold Leaf: "Ancient Technology"/Advanced Material. *Adv. Mater.* **2004**, *16*, 1897-1900.

6.   Detsi, E.; Vukovic, Z.; Punzhin, S.; Bronsveld, P. M.; Onck, P. R.; Hosson, J. T. M. D., Fine-Tuning the Feature Size of Nanoporous Silver. *CrystEngComm* **2012**, *14*, 5402-5406.

7.   Pugh, D. V.; Dursun, A.; Corcoran, S. G., Formation of Nanoporous Platinum by Selective Dissolution of Cu from Cu0.75pt0.25. *J. Mater. Res.* **2003**, *18*, 216-221.

8.   Qi, Z.; Zhao, C.; Wang, X.; Lin, J.; Shao, W.; Zhang, Z.; Bian, X., Formation and Characterization of Monolithic Nanoporous Copper by Chemical Dealloying of Al−Cu Alloys. *J. Phys. Chem. C* **2009**, *113*, 6694-6698.

9.   Zhang, Z.; Wang, Y.; Qi, Z.; Zhang, W.; Qin, J.; Frenzel, J., Generalized Fabrication of Nanoporous Metals (Au, Pd, Pt, Ag, and Cu) through Chemical Dealloying. *J. Phys. Chem. C* **2009**, *113*, 12629-12636.

10.   Hu, K.; Lan, D.; Li, X.; Zhang, S., Electrochemical DNA Biosensor Based on Nanoporous Gold Electrode and Multifunctional Encoded DNA−Au Bio Bar Codes. *Anal. Chem.* **2008**, *80*, 9124-9130.

11.   Xiao, X.; Wang, M. e.; Li, H.; Si, P., One-Step Fabrication of Bio-Functionalized Nanoporous Gold/Poly(3,4-Ethylenedioxythiophene) Hybrid Electrodes for Amperometric Glucose Sensing. *Talanta* **2013**, *116*, 1054-1059.

12. Lang, X. Y.; Yuan, H. T.; Iwasa, Y.; Chen, M. W., Three-Dimensional Nanoporous Gold for Electrochemical Supercapacitors. *Scripta Mater.* **2011**, *64*, 923-926.

13. Cortie, M. B.; Maaroof, A. I.; Stokes, N.; Mortari, A., Mesoporous Gold Sponge. *Aust. J. Chem.* **2007**, *60*, 524-527.

14. Simon, P.; Gogotsi, Y., Materials for Electrochemical Capacitors. *Nat. Mater.* **2008**, *7*, 845-854.

15. Largeot, C.; Portet, C.; Chmiola, J.; Taberna, P.-L.; Gogotsi, Y.; Simon, P., Relation between the Ion Size and Pore Size for an Electric Double-Layer Capacitor. *J. Am. Chem. Soc.* **2008**, *130*, 2730-2731.

16. Hakamada, M.; Mabuchi, M., Thermal Coarsening of Nanoporous Gold: Melting or Recrystallization. *J. Mater. Res.* **2009**, *24*, 301-304.

17. Dursun, A.; Pugh, D. V.; Corcoran, S. G., Dealloying of Ag-Au Alloys in Halide-Containing Electrolytes: Affect on Critical Potential and Pore Size. *J. Electrochem. Soc.* **2003**, *150*, B355-B360.

18. Sharma, A.; Bhattarai, J. K.; Alla, A. J.; Demchenko, A. V.; Stine, K. J., Electrochemical Annealing of Nanoporous Gold by Application of Cyclic Potential Sweeps. *Nanotechnology* **2015**, *26*, 085602.

19. Dorofeeva, T. S.; Seker, E., Electrically Tunable Pore Morphology in Nanoporous Gold Thin Films. *Nano Res.* **2015**, *8*, 2188-2198.

20. Arnob, M. M. P.; Zhao, F.; Zeng, J.; Santos, G. M.; Li, M.; Shih, W.-C., Laser Rapid Thermal Annealing Enables Tunable Plasmonics in Nanoporous Gold Nanoparticles. *Nanoscale* **2014**, *6*, 12470-12475.

21. Schade, L.; Franzka, S.; Mathieu, M.; Biener, M. M.; Biener, J.; Hartmann, N., Photothermal Laser Microsintering of Nanoporous Gold. *Langmuir* **2014**, *30*, 7190-7197.

22.   Seker, E.; Berdichevsky, Y.; Begley, M.; Reed, M.; Staley, K.; Yarmush, M., The
       Fabrication of Low-Impedance Nanoporous Gold Multiple-Electrode Arrays for Neural
       Electrophysiology Studies. *Nanotechnology* **2010**, *21*, 125504.

23.   Daggumati, P.; Matharu, Z.; Seker, E., Effect of Nanoporous Gold Thin Film Morphology
       on Electrochemical DNA Sensing. *Anal. Chem.* **2015**, *87*, 8149-8156.

24.   Senior, N.; Newman, R., Synthesis of Tough Nanoporous Metals by Controlled
       Electrolytic Dealloying. *Nanotechnology* **2006**, *17*, 2311-2316.

25.   Lee, D.; Wei, X.; Chen, X.; Zhao, M.; Jun, S.; Hone, J.; Herbert, E.; Oliver, W.; Kysar, J.,
       Microfabrication and Mechanical Properties of Nanoporous Gold at the Nanoscale.
       Scripta Mater. **2007**, *56*, 437-440.

26.   Chapman, C. A. R.; Chen, H.; Stamou, M.; Biener, J.; Biener, M. M.; Lein, P. J.; Seker,
       E., Nanoporous Gold as a Neural Interface Coating: Effects of Topography, Surface
       Chemistry, and Feature Size. *ACS Appl. Mater. Interfaces* **2015**, *7*, 7093-7100.

27.   Kurtulus, O.; Daggumati, P.; Seker, E., Molecular Release from Patterned Nanoporous
       Gold Thin Films. *Nanoscale* **2014**, *6*, 7062 - 7071.

28.   Tan, Y. H.; Davis, J. A.; Fujikawa, K.; Ganesh, N. V.; Demchenko, A. V.; Stine, K. J.,
       Surface Area and Pore Size Characteristics of Nanoporous Gold Subjected to Thermal,
       Mechanical, or Surface Modification Studied Using Gas Adsorption Isotherms, Cyclic
       Voltammetry, Thermogravimetric Analysis, and Scanning Electron Microscopy. *J. Mater.
       Chem.* **2012**, *22*, 6733-6745.

29.   Kharintsev, S. S.; Noskov, A. I.; Hoffmann, G. G.; Loos, J., Near-Field Optical Taper
       Antennas Fabricated with a Highly Replicable Ac Electrochemical Etching Method.
       Nanotechnology **2011**, *22*, 025202.

30.   Ren, B.; Picardi, G.; Pettinger, B., Preparation of Gold Tips Suitable for Tip-Enhanced
       Raman Spectroscopy and Light Emission by Electrochemical Etching. *Rev. Sci. Instrum.*
       2004, *75*, 837-841.

31.   Qian, G.; Saha, S.; Lewis, K. M., Note: A Simple, Convenient, and Reliable Method to

Prepare Gold Scanning Tunneling Microscope Tips. *Rev. Sci. Instrum.* **2010**, *81*,

016110.

32.   Nichols, R. J.; Magnussen, O. M.; Hotlos, J.; Twomey, T.; Behm, R. J.; Kolb, D. M., An

in-Situ Stm Study of Potential-Induced Changes in the Surface Topography of Au(100)

Electrodes. *J. Electroanal. Chem. Interfacial. Electrochem.* **1990**, *290,* 21-31.

33.   Erlebacher, J., Mechanism of Coarsening and Bubble Formation in High-Genus

Nanoporous Metals. *Phys. Rev. Lett.* **2011**, *106*, 225504.

34.   Chen-Wiegart, Y.-c. K.; Wang, S.; Chu, Y. S.; Liu, W.; McNulty, I.; Voorhees, P. W.;

Dunand, D. C., Structural Evolution of Nanoporous Gold During Thermal Coarsening.

Acta Mater. **2012**, *60*, 4972-4981.

35.   Kertis, F.; Snyder, J.; Govada, L.; Khurshid, S.; Chayen, N.; Erlebacher, J.,

Structure/Processing Relationships in the Fabrication of Nanoporous Gold. *JOM-J. Min.*

Met. Mat. S. **2010**, *62*, 50-56.

36.   Qi, Z.; Weissmüller, J., Hierarchical Nested-Network Nanostructure by Dealloying. *ACS*

Nano **2013**, *7*, 5948-5954.

1
2
3
4
5
6
7
8
9
10
11
12
13
14
15
16
17
18
19
20
21
22
23
24
25
26
27
28
29
30
31
32
33
34
35
36
37
38
39
40
41
42
43
44
45
46
47
48
49
50
51
52
53
54
55
56
57
58
59
60

TABLE OF CONTENTS IMAGE